Interfacial Interactions of a Novel Mechanochemical Composite of Cellulose with Maleated Polypropylene

Wulin Qiu, Takashi Endo, Takahiro Hirotsu

National Institute of Advanced Industrial Science and Technology (AIST), 2217-14 Hayashi-cho, Takamatsu 761-0395, Japan

Received 27 October 2003; accepted 4 June 2004
DOI 10.1002/app.21123
Published online in Wiley InterScience (www.interscience.wiley.com).

ABSTRACT: A novel composite was prepared by ball-milling crystalline cellulose and maleic anhydride (MA) grafted polypropylene (MAPP) and its characteristics compared with a corresponding composite prepared by a conventional melt-mixing method. The ball-milling induces the formation of more ester bonds between cellulose and MAPP. The resulting MAPP chains bound to particles of cellulose, which created much stronger interfacial adhesion between the cellulose particles and the MAPP matrix. Accordingly, such enhanced interfacial adhesion substantially differentiates the mechanochemically prepared composite from the melt-mixed composite. © 2004 Wiley Periodicals, Inc. J Appl Polym Sci 94: 1326–1335, 2004

Key words: poly(propylene) (PP); polysaccharides; interfaces; composites; mechanical properties

INTRODUCTION

Cellulose is the most abundant natural polymer, with as much as 300 billion tons a year formed on earth. Because of its renewability, biodegradability, and nontoxicity, increasing attention has been paid to the use of cellulosic materials for novel composites.[1–15] However, the inherent incompatibility of hydrophilic cellulose fibers with hydrophobic thermoplastic polyolefin inhibits good adhesion between cellulose and the matrix, making the composites impractical.

The properties of such composites depend on their interfacial adhesion as well as the properties of the individual components. Many studies have been performed to enhance the interfacial adhesion,[1,3,11,15–21] and it has been found that maleic anhydride (MA) grafted polypropylene (MAPP) is very efficient for preparing cellulosic PP composites with improved mechanical properties. The improvement imparted by the use of MAPP is considered to be attributed to ester bond formation between the maleic anhydride groups of MAPP and the hydroxyl groups of cellulose. The esterification in solutions in the presence of a catalyst has been confirmed by the appearance of a new IR band at 1729 to 1750 cm^{-1}.[22–26] However, no direct evidence of esterification has been demonstrated from the melt-mixing of cellulosic materials with MAPP, although the relevant composites are generally prepared by a melt-mixing method. This implies that highly crystalline cellulose is too stable to form a number of ester bonds with MAPP in a melted state, because it possesses very few free OH groups because of extensive formation of hydrogen bonds.[27,28]

For melt-mixed composites of crystalline cellulose and PP compatibilized with MAPP, even an amount of grafted MA as small as 0.2 wt % is sufficient to impart maximum mechanical properties to the resulting composites.[29,30] This result is in agreement with the limited esterification between crystalline cellulose and MAPP. Recently, however, we have found that ball-milling induces intensive esterification between the OH groups on microparticles of cellulose and the MA groups of MA grafted polyethylene (MAPE),[31] or MAPP,[32] in marked contrast to the melt-mixing of the original cellulose and MAPE or MAPP, in which the number of ester bonds is too few to be observed by FTIR spectroscopy.[32] The composites prepared by ball-milling first exhibit tensile properties different from those prepared by melt-mixing alone, suggesting that the MAPE or MAPP chains bound to the cellulose determine the interfacial structure of the resultant composite. However, the nature and structure of the interface has not yet been clarified. In this study, we describe in detail the structure and thermal properties of MAPP chains bound to microparticles of cellulose, which are derived from a composite prepared by ball-milling highly crystalline cellulose and MAPP, and demonstrate that the nature of the bound MAPP chains determines the interfacial structure and, accordingly, the tensile property of the composite.

Correspondence to: T. Hirotsu (takahiro-hirotsu@aist.go.jp).

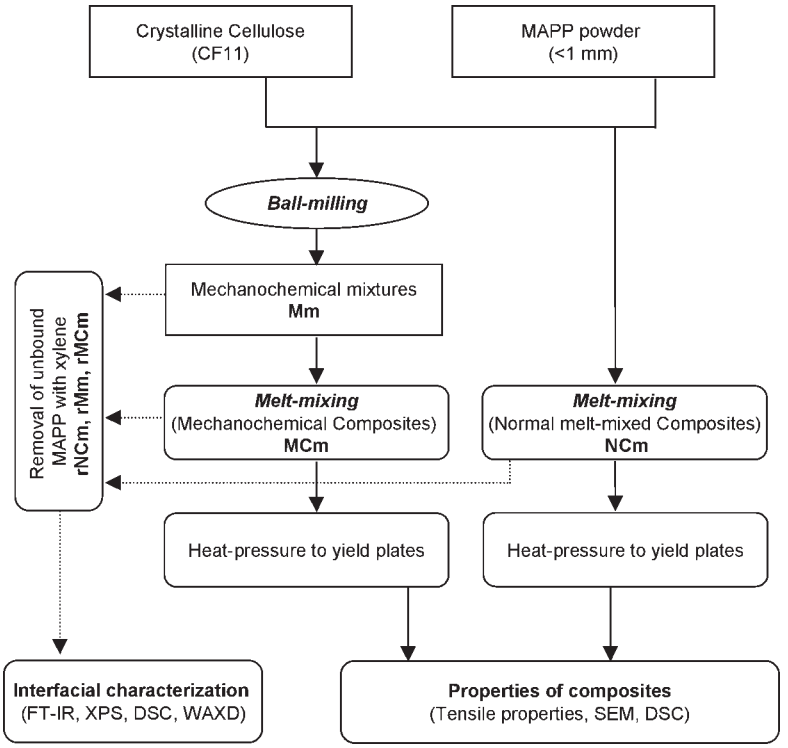

Scheme 1

EXPERIMENTAL

Materials

MAPP pellets [MA content: ~ 0.6 wt %, melt flow index: 115 g/10 min (190°C, 2.16 kg, ASTM D 1238), and density: 0.950 g/cm^3, from http://www.sigma-aldrich.com] were obtained from Aldrich Chemical Co. (Milwaukee, WI). Fibrous cellulose [CF11; 50–350 μm in length, about 20 μm in diameter, and 93% in crystallinity (cellulose I type)[33,34]] was purchased from Whatman International, Ltd. (Kent, UK).

Preparation of composites

CF11 was dried *in vacuo* at 60°C for 48 h. MAPP pellets were pulverized to a size smaller than 1 mm, and pretreated *in vacuo* at 120°C for 12 h before use. Composites with different constituent ratios of CF11/MAPP were prepared by two methods as shown in Scheme 1.

One is the normal melt-mixing method with a Labo Plastomill 30C150 Rheomix apparatus (volume of the mixing chamber: 60 cm^3; Toyoseiki Kogyo, Tokyo, Japan). The mixing process with a sample weight of 40 g was carried out at 190°C and 75 rpm for 20 min. The relevant composite is denoted as NCm, where m indicates the cellulose content (wt %) in the composite. The other is a mechanochemical method we developed: CF11 and MAPP were ball-milled together for a certain time, followed by the same melt-mixing step. The ball-milling process was performed in a Planetary Ball Mill (Pulverisette 5, Fritsch, Germany) equipped with four jars, each 500 cm^3 in volume and loaded with 25 balls (diameter: 1.5 cm). The sample (45 g) in each jar was milled at a rotational speed of 250 rpm, with a cyclic mode of 50-min milling followed by a 10-min pause, repeated for 8 h. The mixture obtained from the ball-milling process only is denoted as Mm, and the composite obtained by the full mechanochemical method is denoted as MCm, where m has the same meaning as above.

Plates of 1 mm thickness were obtained by compression-molding of the composites with a Shinto press (Shinto Metal Industries, Japan), at 200°C at a pressure of 3 MPa for 6 min, followed by cooling to room temperature at a fixed cooling speed under a pressure of 7 MPa. The plates were cut into a standard shape for the testing of tensile properties.

Removal of unbound MAPP from the products

A small amount of each product (NC30 and MC30) was independently pulverized with the aid of liquid nitrogen, and dried at 60°C *in vacuo* to a constant mass. Approximately 3 g of each powder (and also M30) was extracted in a Soxhlet extractor with xylene at 160°C for 48 h to remove the unbound MAPP. The residual powder was dried *in vacuo* at 120°C for 12 h before measuring the weight of the MAPP bound to the cellulose. The residual samples are denoted as rNC30,

rM30, and rMC30, respectively. Samples of neat MAPP and neat cellulose were also treated by the same method, for reference purposes.

FTIR analysis

FTIR spectra of rNC30, rM30, and rMC30 were recorded by a KBr technique on a Perkin–Elmer 2000 spectrometer (Perkin Elmer Cetus Instruments, Norwalk, CT) at a resolution of 4 cm^{-1} in the range of 4000–400 cm^{-1} for 300 scans.

X-ray photoelectron spectroscopy (XPS)

XPS spectra of rNC30, rM30, and rMC30 were recorded on a Shimadzu ESCA-K1 electron spectrometer (Shimadzu, Kyoto, Japan) with a monochromated magnesium–K_α (1253.6 eV) X-ray source at an energy resolution of 16 eV.

Differential scanning calorimetry (DSC)

DSC measurements were performed with a Perkin–Elmer DSC 7 instrument in a nitrogen atmosphere. Samples were held at 230°C for 3 min, then cooled to 50°C at a rate of −10°C/min, maintained at 50°C for 3 min, and then reheated to 230°C at a rate of 10°C/min. The DSC behaviors during the cooling and the second heating were recorded.

Wide-angle X-ray diffraction (WAXD)

WAXD measurements were carried out with a Rigaku RINT-2100 X-ray diffractometer (Rigaku, Tokyo, Japan), using a Cu–K_α radiation (40 kV, 24 mA).

Scanning electron microscopy (SEM)

The morphology of the NCm and MCm composites was examined using an S-2 460N electron microscope (Hitachi, Osaka, Japan) at 25 kV. The plates of the composites were fractured in liquid nitrogen and the fractured surfaces were sputter-coated with gold–palladium alloy before viewing.

Tensile tests

Tensile properties were measured with a Shimadzu AGS-5kNG universal testing machine in accordance with the testing method for tensile properties of plastics (at a strain speed of 5 mm/min).[35] The composite plates were stored in a room with a constant temperature of 20°C and a constant humidity of 65% for over 48 h, before the measurement. Each result was the average taken from six parallel tests.

RESULTS AND DISCUSSION

We consider that mechanochemical esterification between cellulose and MAPP is essential for compounding of hydrophilic cellulose with hydrophobic PP because the bound MAPP chains can probably interact with PP chains in the matrix. The esterification is demonstrated and the MAPP chains bound to cellulose particles are characterized by using the residual samples, rMC30, rM30, and rNC30. Then, the distinction between the MC and NC composites is discussed with respect to the properties of the bound MAPP chains.

Chemical bonding of MAPP chains to microparticles of cellulose

The extraction residues rNC30, rM30, and rMC30 exhibited weight increases of 2.1, 10.9, and 23.8 wt %, respectively, compared with that of the cellulose content. The increase shows that MAPP chains are bound to the cellulose particles, given that the same solvent extractions of neat MAPP and CF11 yield weight losses of 100 and 0 wt %, respectively. The contents of bound MAPP (based on the weight of initial MAPP in the composite) are 0.9 wt % for NC30, 4.7 wt % for M30, and 10.2 wt % for MC30. This indicates that the ball-milling enables more MAPP chains to bind to cellulose in the composite.

FTIR spectra of the extraction residues are shown in Figure 1, compared with those of MAPP and CF11. Before describing the results from the residues, we note the characteristics of MAPP and cellulose. MAPP exhibits a broad absorption centered at 1786 cm^{-1} (symmetric Cdbond]O stretching) in Figure 1(f), which indicates that MA monomers are grafted principally at the end of a PP chain to form a single (1792 cm^{-1}) or an oligomeric graft (1784 cm^{-1}).[36,37] Although the melt-mixing of MAPP causes hardly any change in the IR pattern [Fig. 1(g)], the ball-milling causes a decrease in absorption strength at 1792 cm^{-1} and further yields a new band at about 1560 cm^{-1} [Fig. 1(h) and (i)]. Because the MAPP sample contains a slight amount of CaO (found from http://www.sigma-aldrich.com), the activated CaO may react with grafted MA groups of the MAPP to form carboxylates.[38] The decrease in absorption strength at 1792 cm^{-1} indicates that the single grafts are more reactive than the oligomeric grafts.

The ball-milling of CF11 causes the broadening of the bands, except for the band at 898 cm^{-1} that reflects changes in molecular conformation attributed to the antisymmetric out-of-phase ring stretching.[27] It is noted that the OH stretching band shifts from 3340 to 3400 cm^{-1} with the ball-milling. This means that a network of hydrogen bonds in the original CF11 is collapsed mechanochemically to yield free OH groups on the cellulose microparticles.

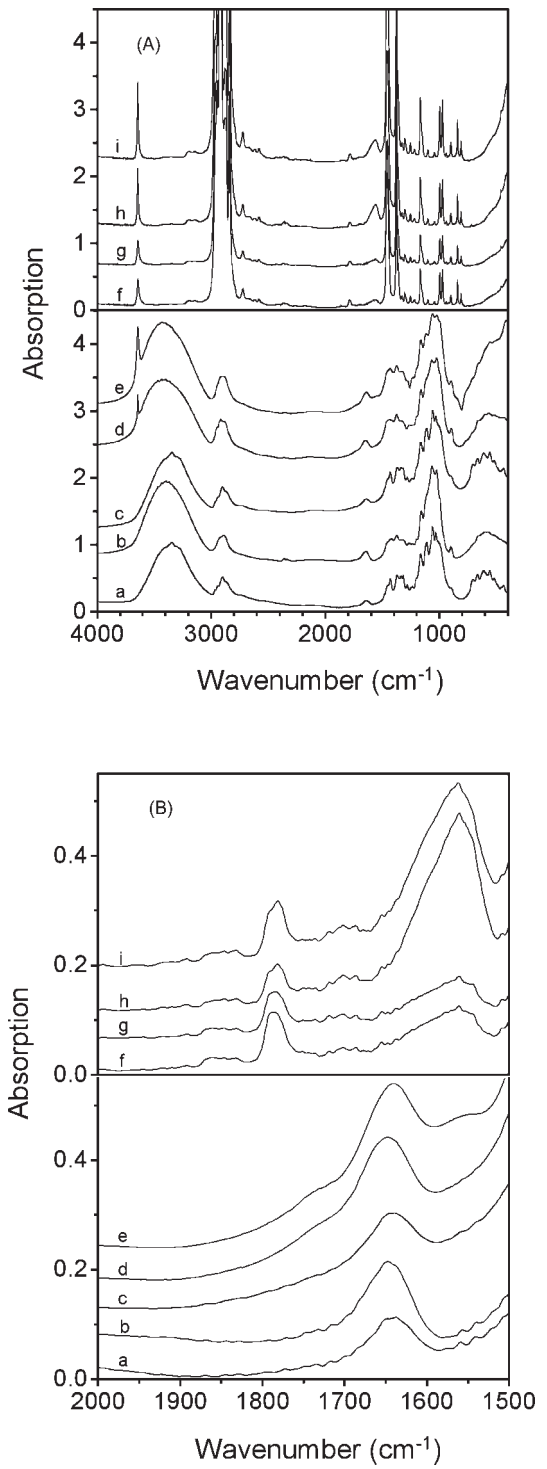

Figure 1 FTIR spectra of (a) CF11, (b) milled CF11, (c) rNC30, (d) rM30, (e) rMC30, (f) MAPP, (g) melt-mixed MAPP, (h) milled MAPP, and (i) milled then melt-mixed MAPP. (B) is a magnification of (A).

A comparison of Figure 1(c) with Figure 1(a) reveals that the spectrum of rNC30 is almost the same as that of the original CF11. Quite unlike rNC30, rM30 and rMC30 reveal a new shoulder around 1730 cm^{-1}, which is assigned to ester bonds.[32] This indicates that the esterification occurs much more frequently between cellulose and MAPP by the ball-milling than by melt-mixing alone.

XPS is very useful for characterizing the quantitative elemental composition and functional groups of the surface of a substance to a depth of about 1–10 Å.[39] Figure 2 shows XPS spectra of the extraction residues rNC30, rM30, and rMC30, together with the results for CF11 and MAPP. The peak–area ratios of carbon (C 1s) to oxygen (O 1s) are 1.12 for rNC30, 1.60 for rM30, and 2.05 for rMC30, with 0.76 (0.70) for original (milled) CF11 and 1.78 for MAPP. It is noted that the residues exhibit greater C/O ratios than that of cellulose and that the ratio for rMC30 is greater than that for MAPP, in the order of cellulose $<$ rNC30 $<$ rM30 $<$ MAPP $<$ rMC30.

The greater C/O ratios for the residues than for CF11 mean that cellulose fibers/particles are covered by MAPP chains because of the greater C/O ratio for MAPP than for CF11 (Fig. 2). Furthermore, the order of the C/O ratios for the residues is consistent with that of the weight increases described earlier. Accordingly, esterification between cellulose and MAPP probably occurs in NC30, as well as in M30 and MC30, although the esterification was not confirmed in rNC30 by FTIR.

The XPS results demonstrate that esterification occurs on the surface of the cellulose fibers/particles in rNC30, rM30, and rMC30. A molecular chain of MAPP has an MA single or MA oligomeric graft at the end of the PP chain, on the basis of the IR results.[36,37] Thus, surface esterification causes the PP chain side of MAPP chains bound to a cellulose particle to stretch out from the surface of the particle. This produces a core–shell structure: the core is a cellulose particle and the shell is composed of long hydrophobic PP chains stretching out from the core. This structure is consistent with the greater C/O ratio for rMC30 than for MAPP because the C/O ratio of MAPP reflects the average constitution of a MAPP chain.

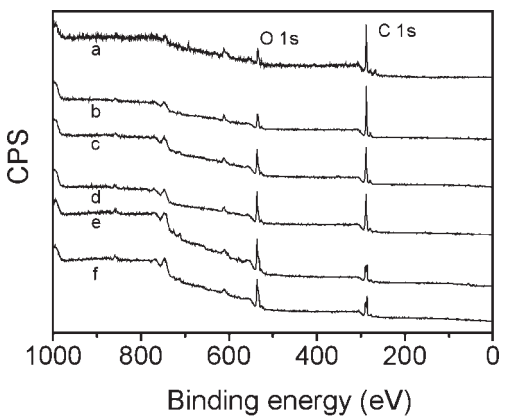

Figure 2 XPS spectra of (a) MAPP, (b) rMC30, (c) rM30, (d) rNC30, (e) milled CF11, and (f) original CF11.

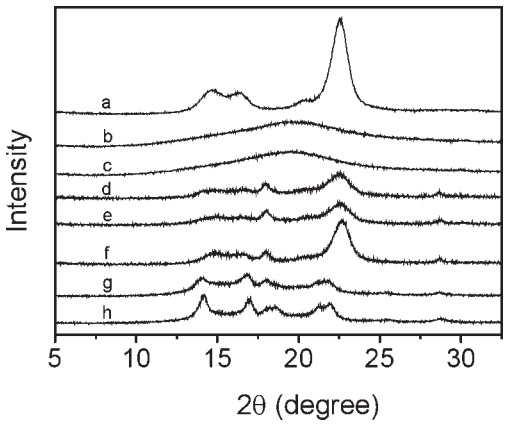

Figure 3 WAXD patterns of (a) original CF11, (b) milled CF11, (c) milled and xylene-treated CF11, (d) rMC30, (e) rM30, (f) rNC30, (g) milled then melt-mixed MAPP powder, and (h) melt-mixed MAPP powder.

Nature of MAPP chains bound to particles of cellulose

The crystallinity of the MAPP bound to the cellulose particles in the extraction residues is confirmed directly by X-ray diffraction. CF11 is an I-type cellulose with reflections: (101) at $2\theta = 14.7°$, ($10\bar{1}$) at $2\theta = 16.3°$, (021) at $2\theta = 20.4°$, and (002) at $2\theta = 22.7°$ [Fig. 3(a)].[40] The ball-milling of the original CF11 causes its transformation into an amorphous state [Fig. 3(b)]. MAPP belongs to the monoclinic α-form with reflections: (110) at $2\theta = 14.2°$, (040) at $2\theta = 17.0°$, (130) at $2\theta = 18.6°$, (111) at $2\theta = 21.3°$, and (-131) at $2\theta = 22.0°$ in Figure 3(h),[41,42] where reflections at $2\theta = 18.2$ and 28.7° are assigned to $Ca(OH)_2$,[43] a hydrolysis product of CaO. The ball-milling of MAPP results in a reflection shift by $-0.1°$ for (110) and (111) and by -0.2 ° for (040) and (-131), whereas the reflection (130) at $2\theta = 18.6°$ changes into a very small shoulder [Fig. 3(g)]. Compared with the results for CF11 and MAPP, rM30 and rMC30 reveal very weak reflections attributed to the bound MAPP: (110) and (040) as well as a reduced reflection assigned to cellulose (002) compared to the reflection for rNC30 [Fig. 3(d)–(f)]. It is noted from a comparison of Figures 3(b) and 3(c) that the xylene extraction has no effect on the crystallinity of the milled CF11. The higher crystallinity for cellulose in rM30 and rMC30 than that for milled CF11 suggests that the cellulose particles are covered by the bound MAPP chains and, accordingly, are protected from the outer forces.

DSC profiles of rNC30, rM30, and rMC30 are shown in Figure 4 and are contrasted with the results of CF11 and MAPP. Cellulose is stable under experimental conditions.[29] In Figure 4(Aa), the endothermic peak at about 100°C is attributed to the desorption of physically adsorbed H_2O; this peak shifts to a higher temperature after the ball-milling [Fig. 4(Ab)]. This probably results from the formation of hydrogen bonds between H_2O molecules and activated OH groups of cellulose after the ball-milling. No peak is observed in Figure 4(Ba) and (Bb) because of the slow adsorption of H_2O. Accordingly, the peaks for rNC30, rM30, and rMC30 result from the MAPP chains bound to the cellulose particles.

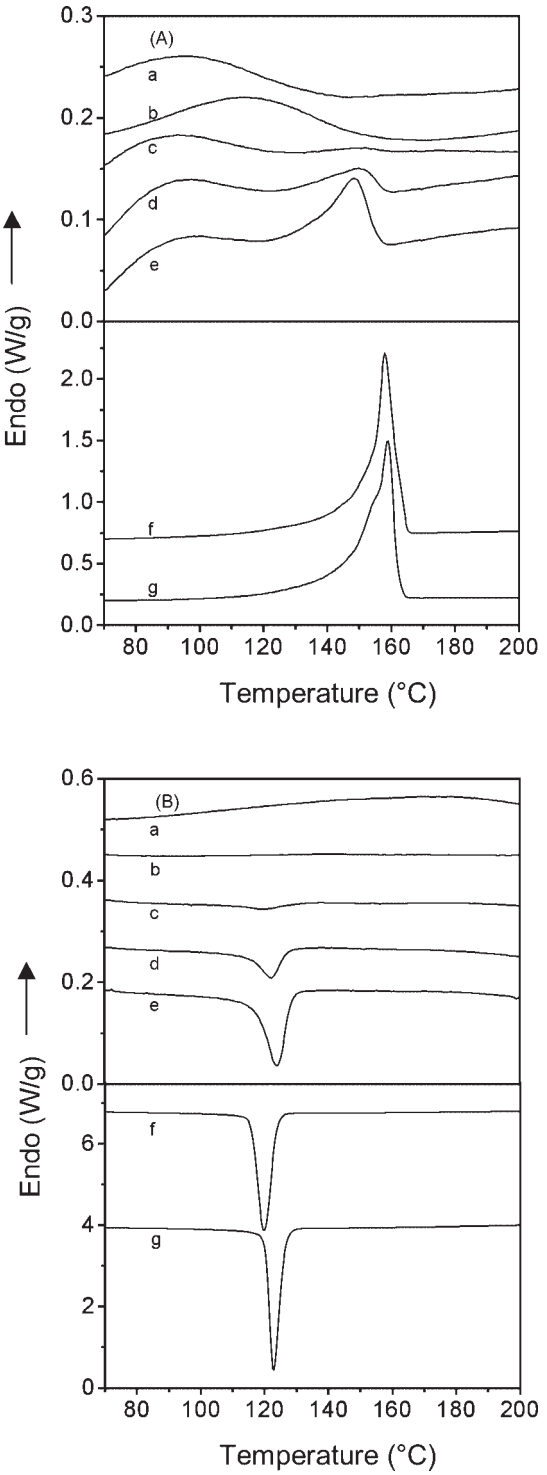

Figure 4 DSC curves of heating (A) and cooling (B) of (a) original CF11, (b) milled CF11, (c) rNC30, (d) rM30, (e) rMC30, (f) melt-mixed MAPP powder, and (g) milled then melt-mixed MAPP powder.

TABLE I
DSC Characteristics of MAPP Chains Bound to Cellulose in rNC30, rM30, and rMC30

Sample	Crystallization		Melting	
	Temperature[a] (°C)	ΔH_c[b] (J/g)	Temperature[a] (°C)	ΔH_m[b] (J/g)
MAPP				
Melt-mixing	120	−92.4	158	93.8
Milled/melt-mixing	123	−90.6	159	91.7
rNC30	120	−34.2	150	17.1
rM30	122	−37.0	150	24.1
rMC30	124	−45.3	148	30.0

[a] The value corresponds to the center of each DSC peak.
[b] The value is calculated on the basis of the weight of bound MAPP for rNC30, rM30, and rMC30.

The crystallization and melting behaviors of the MAPP chains bound to cellulose particles in rNC30, rM30, and rMC30 are summarized along with those for MAPP in Table I, where the enthalpies for crystallization and melting, ΔH_c and ΔH_m, are based on the unit weight of the bound MAPP. It is very interesting that the values of ΔH_c and ΔH_m increase in the order of rNC30 < rM30 < rMC30, although these values are all much smaller than those of MAPP. The enthalpies reflect the crystalline phase of MAPP chains. Accordingly, the above result also demonstrates that the MAPP chains bound to the cellulose particles in rNC30, rM30, and rMC30 can crystallize, even though the degree of crystallinity is much smaller for the residues than that for MAPP itself. Furthermore, the result shows that the MAPP chains bound to the particles of cellulose crystallize more extensively with an increase in the number of bound MAPP chains, probably because of more and/or stronger intermolecular interactions. This indicates that the bound MAPP chains can crystallize not only within themselves but also with each other. The intermolecular crystallization of the bound MAPP strongly suggests adhesion between cellulose particles and the MAPP matrix, given that the bound MAPP chains can cocrystallize with the unbound MAPP chains in the matrix, acting as a compatibilizer.

The melting temperatures of the residues are lower than that of MAPP, but there is almost no change in crystallization temperature between the residues and MAPP, as shown in Table I. The decrease in melting temperature may indicate the formation of smaller crystallites for the bound MAPP chains than for original MAPP, as well as roughness in assembly of the bound MAPP chains in close proximity to the cellulose particles.

A model of MAPP-bound particles of cellulose

On the basis of the characteristics of the residues rNC30, rM30, and rMC30 after xylene extraction of the corresponding composites, we have demonstrated that the ball-milling of crystalline cellulose with MAPP induces the formation of more ester bonds between OH groups on the resulting amorphous particles of cellulose and MA groups of MAPP (rM30 and rMC30), quite unlike the case of melt-mixing alone (rNC30), in which the cellulose retains high crystallinity. The XPS analysis of the C/O ratio for the residues reveals that the cellulose particles bind the MA grafts at the end of MAPP chains, with the hydrophobic hydrocarbon sides stretching out from the core of cellulose. It is of great interest that the MAPP chains bound to the cellulose particles crystallize with each other as well as in themselves, the extent of crystallinity increasing with the number of bound MAPP chains, even though the crystallinity is much smaller than that of neat MAPP.

The above characterization makes it possible to construct a model of the cellulose particles bound with MAPP chains, the MA grafting end forming an ester bond to a cellulose particle and the other hydrocarbon end stretching out, forming a core–shell structure (Fig. 5). The hydrocarbon chains stretching out from the core particle of cellulose can interact strongly with a matrix consisting of PP chains through cocrystallization and/or entanglement and, accordingly, most likely confer strong interfacial adhesion between the cellulose particle and the matrix. Furthermore, the interaction may realize good distribution of such microparticles of cellulose in the matrix. Therefore, we can expect that the substantial improvement in interfacial adhesion and improved distribution of cellulose particles in a PP matrix will raise the tensile strength of the resultant cellulose composite with MAPP, and thus MC composites prepared by the ball-milling method will exhibit higher tensile strengths than those of the corresponding NC composites prepared by the usual melt-mixing method, despite the smaller cellulose particle size in the former.

Distinctions between MC and NC composites

Interfacial adhesion

SEM micrographs of fractured surfaces of the composites MC and NC are shown in Figure 6. Much im-

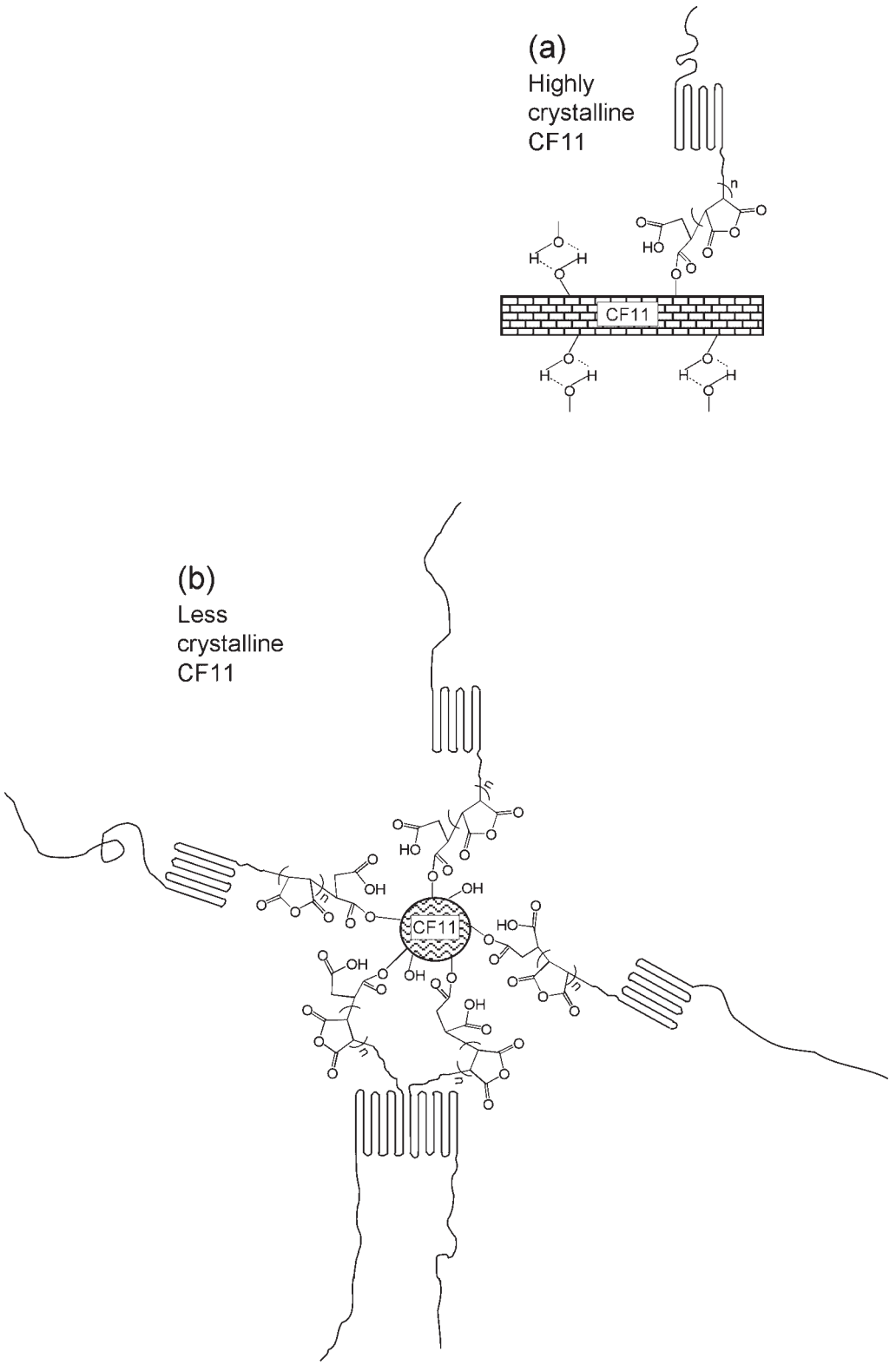

Figure 5 Model of the MAPP chains bound to a cellulose particle in (a) NC and (b) MC composites.

proved distribution of particles of cellulose can be found in the MCs, in contrast to the NCs. The magnified micrographs of NC30 [Fig. 6(e)] and MC30 [Fig. 6(f)] reveal a marked difference in interfacial adhesion between cellulose particles and the MAPP matrix. For the NC30, a fibrous particle of cellulose is partially covered by the MAPP matrix, with a part of the surface still naked, as shown in Figure 6(e). This proves

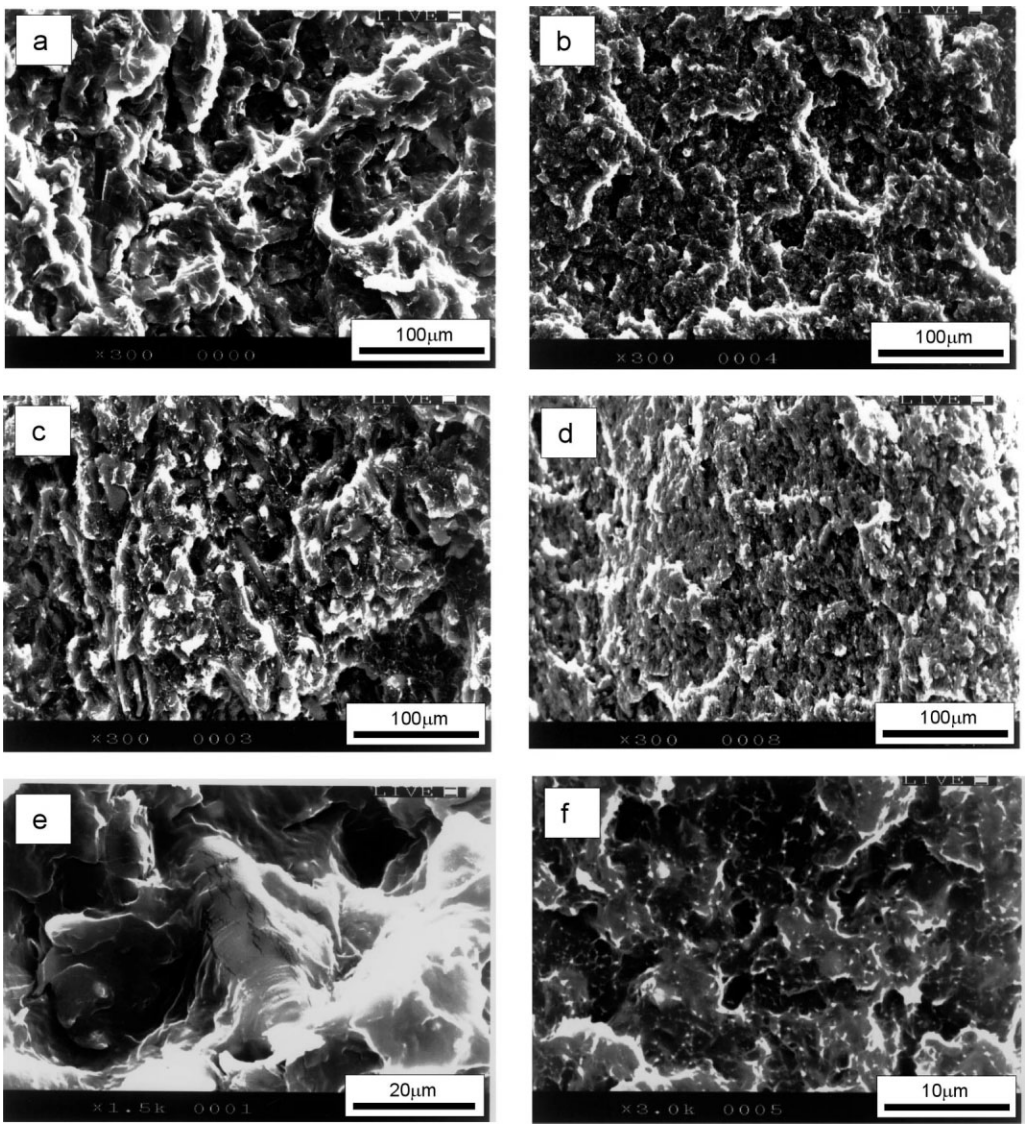

Figure 6 SEM microphotographs of fractured surfaces of NC30 (a: ×300; e: ×1500), MC30 (b: ×300; f: ×3000), NC60 (c: ×300), and MC60 (d: ×300).

that the interfacial interactions are limited in the NC composites prepared through the normal melt-mixing method, probably because of a smaller number of ester bonds between highly crystalline cellulose and the MAPP matrix. For the MC30, by contrast, it is difficult to differentiate cellulose particles from the MAPP matrix [Fig. 6(f)]. The cellulose particles are tightly covered with the MAPP matrix. This indicates stronger interfacial interactions as a result of more MAPP chains bound to the cellulose particles in the MC composites, consistent with the aforementioned model.

Melting and crystallization behavior

The melting behaviors of the MC and NC composites are almost the same as that of neat MAPP, and not dependent on the cellulose content, as shown in Figure 7(A). However, the crystallization behaviors of the composites are certainly different, depending on the cellulose content [Fig. 7(B)].

The peak temperatures of crystallization (T_c), for the MC and NC composites are plotted against the cellulose content in Figure 8(A). The T_c values of the MC and NC composites increase with increasing cellulose content; the value for MC is greater than that for NC for a cellulose content less than 70 wt %. Cellulose particles can act as an nucleating agent for the crystallization of MAPP, and consequently increase the crystallization temperature as well as the crystallization rate of MAPP.[17,29] The supercooling ($T_m - T_c$) of MC is smaller than that of NC for a cellulose content within 70 wt %, where T_m denotes the melting temperature. This suggests that the nucleation effect of

cellulose particles in MC is much greater than that in NC. Such enhanced nucleation may result from the stronger interfacial adhesion between cellulose and MAPP in the MC than in the NC composite.

Tensile properties

Increases in tensile strength as well as in Young's modulus with increasing cellulose content can be found in both MC and NC composites, as shown in Figure 9. It is very interesting that the MC composite shows a greater tensile strength than that of the NC, with almost no difference in Young's modulus. The elongation at breaking point of the MC and NC composites decreased very slightly with an increase in the cellulose content, in agreement with previous results.[29] This may be attributable to a very small elongation of the original MAPP (~ 5%). Compared with the NC composite, the marked increase in tensile strength for the MC composite is undoubtedly caused by the improved interfacial adhesion as well as the improved distribution of cellulose particles in the matrix. The improved interfacial adhesion and cellulose distribution can confer the effective transfer of stresses through the interface, resulting in much greater mechanical strength for the MC composite. Accordingly, the enhanced interfacial adhesion of the MC composite compensates for the decrease in tensile strength resulting from the reduction of the aspect ratio of cellulose.

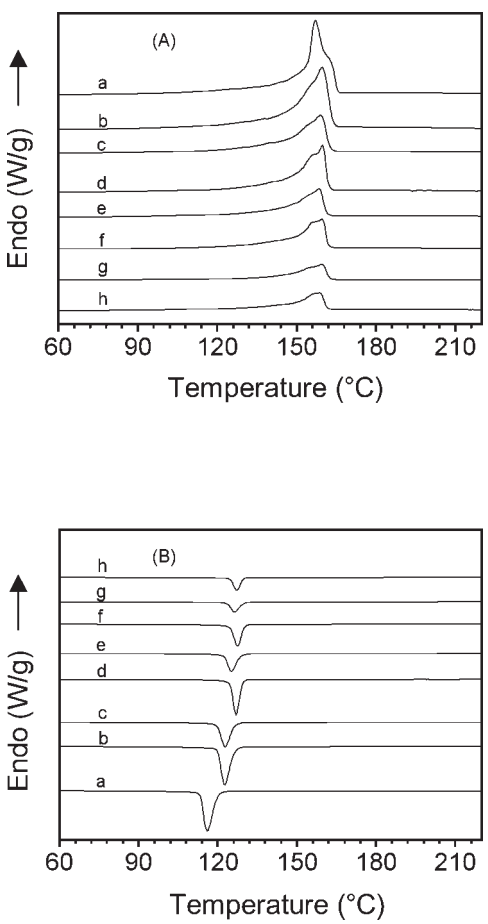

Figure 7 DSC curves of heating (A) and cooling (B) of (a) melt-mixed MAPP, (b) milled then melt-mixed MAPP, (c) NC30, (d) MC30, (e) NC50, (f) MC50, (g) NC70, and (h) MC70.

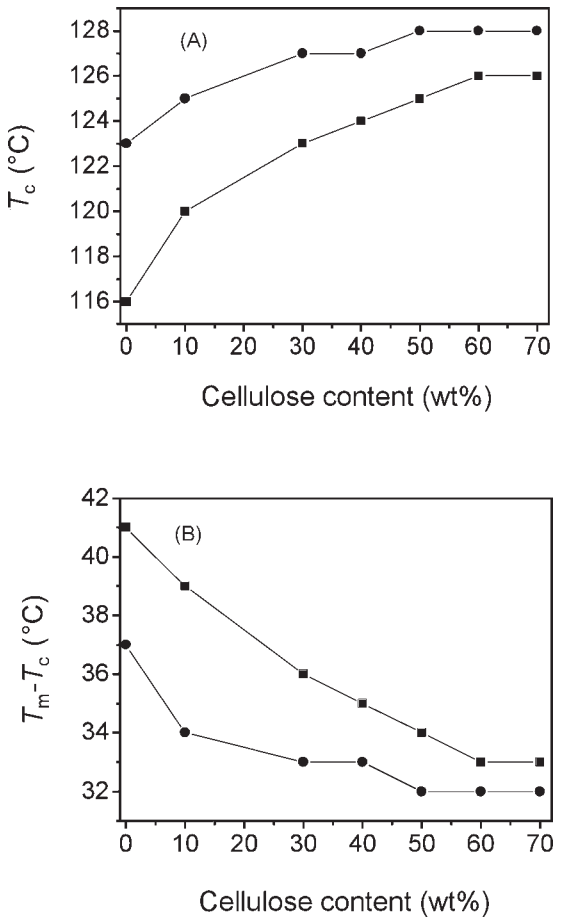

Figure 8 Crystallization temperature (A) and the supercooling (B) are plotted against the cellulose content for NC (■) and MC composites (●).

CONCLUSION

The ball-milling of crystalline cellulose with MAPP induces the formation of more ester bonds between the OH groups on the resulting amorphous cellulose particles and MA groups of MAPP, compared with the case by melt-mixing only. Great numbers of MAPP chains bind to the cellulose particles to form a core–shell structure, creating not only stronger interfacial adhesion between the cellulose particles and the MAPP matrix but also greatly improved distribution of the cellulose particles in the matrix, which in turn results in the greater tensile strength of the MC composite than that of NC.

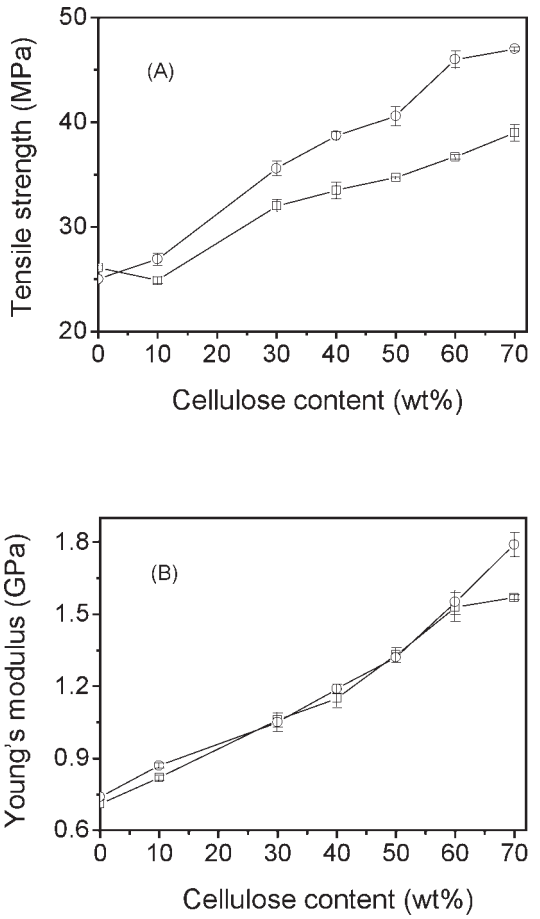

Figure 9 Tensile strength (A) and Young's modulus (B) are plotted against the cellulose content for NC (□) and MC composites (○).

References

1. Aranberri-Askargorta, I.; Lampke, T.; Bismarck, A. J Colloid Interface Sci 2003, 263, 580.
2. Ioelovich, M.; Figovsky, O. Polym Adv Technol 2002, 13, 1112.
3. Yuan, X. W.; Jayaraman, K.; Bhattacharyya, D. J. Adhes Sci Technol 2002, 16, 703.
4. Allan, G. G.; Stoyanov, A. P.; Ueda, M.; Yahiaoui, A. Cellulose 2001, 8, 127.
5. Averous, L.; Fringant, C.; Moro, L. Polymer 2001, 42, 6565.
6. Angles, M. N.; Dufresne, A. Macromolecules 2001, 34, 2921.
7. Curvelo, A. A. S.; de Carvalho, A. J. F.; Agnelli, J. A. M. Carbohydr Polym 2001, 45, 183.
8. Angles, M. N.; Dufresne, A. Macromolecules 2000, 33, 8344.
9. Whitney, S. E. C.; Gidley, M. J.; McQueen-Mason, S. J. Plant J 2000, 22, 327.
10. Chazeau, L.; Cavaille, J. Y.; Perez, J. J Polym Sci Part B: Polym Phys 2000, 38, 383.
11. Snijder, M. H. B.; Bos, H. L. Compos Interface 2000, 7, 69.
12. Takatani, M.; Ito, H.; Ohsugi, S.; Kitayama, T.; Saegusa, M.; Kawai, S.; Okamoto, T. Holzforschung 2000, 54, 197.
13. Dufresne, A.; Kellerhals, M. B.; Witholt, B. Macromolecules 1999, 32, 7396.
14. Zhang, F. R.; Kabeya, H.; Kitagawa, R.; Hirotsu, T.; Yamashita, M.; Otsuki, T. Chem Mater 1999, 11, 1952.
15. Bledzki, A. K.; Gassan, J. Prog Polym Sci 1999, 24, 221.
16. Joseph, P. V.; Joseph, K.; Thomas, S. Compos Interface 2002, 9, 171.
17. Amash, A.; Zugenmaier, P. Polym Bull 1998, 40, 251.
18. Geethamma, V. G.; Mathew, K. T.; Lakshminarayanan, R.; Thomas, S. Polymer 1998, 39, 1483.
19. Gassan, J.; Bledzki, A. K. Composites Part A 1997, 28A, 1001.
20. George, J.; Sreekala, M. S.; Thomas, S. Polym Eng Sci 2001, 41, 1471.
21. Amash, A.; Zugenmaier, P. Polymer 2000, 41, 1589.
22. Matías, M. C.; Orden, de la M. U.; Sánchez, C. G.; Urreaga, J. M. J Appl Polym Sci 2000, 75, 256.
23. Felix, J. M.; Gatenholm, P. J Appl Polym Sci 1991, 42, 609.
24. Yang, C. Q. J Appl Polym Sci 1993, 50, 2047.
25. Kazayawoko, M.; Balatinecz, J. J.; Woodhams, R. T. J Appl Polym Sci 1997, 66, 1163.
26. Baiardo, M.; Frisoni, G.; Scandola, M.; Licciardello, A. J Appl Polym Sci 2002, 83, 38.
27. Dumitriu, S. Polysaccharides: Structural Diversity and Functional Versatility; Marcel Dekker: New York, 1998.
28. Kennedy, J. F.; Phillips, G. O.; Wedlock, D. J.; Williams, P. A. Cellulose and Its Derivatives: Chemistry, Biochemistry and Applications; Ellis Horwood: Chichester, UK, 1985.
29. Qiu, W. L.; Zhang, F. R.; Endo, T.; Hirotsu, T. J Appl Polym Sci 2003, 87, 337.
30. Qiu, W. L.; Endo, T.; Hirotsu, T., to appear.
31. Zhang, F. R.; Qiu, W. L.; Yang, L. Q.; Endo, T.; Hirotsu, T. J Mater Chem 2002, 12, 24.
32. Qiu, W. L.; Zhang, F. R.; Endo, T.; Hirotsu, T. J Appl Polym Sci 2003, 91, 1703.
33. Endo, T.; Kitagawa, R.; Hirotsu, T.; Hosokawa, J. Kobunshi Ronbunshu 1999, 56, 166 (in Japanese).
34. Endo, T.; Zhang, F.; Kitagawa, R.; Hirotsu, T.; Hosokawa, J. Polym J 2000, 32, 182.
35. Japan Standard Society, JIS K7113-1995; Japan Standard Society: Tokyo, 1995.
36. Roover, de. B.; Sclavons, M.; Carlier, V.; Devaux, J.; Legras R.; Momtaz, A. J Polym Sci Part A: Polym Chem 1995, 33, 829.
37. Zhang, F. L.; Endo, T.; Kitagawa, R.; Kabeya H.; Hirotsu, T. J Mater Chem 2000, 10, 2666.
38. Charles, J. P. The Aldrich Library of Infrared Spectra, 3rd ed.; Aldrich Chemical Company: Milwaukee, WI, 1981.
39. Kazayawoko, M.; Balatinecz, J. J.; Woodhams, R. T.; Sodhi, R. N. S. J Wood Chem Technol 1998, 18, 1.
40. Fink, H. P.; Hofmann, D.; Philipp, B. Cellulose 1995, 2, 51.
41. Rajesh, H. S.; Benjamin, S. H.; Aurora, N.; Hitesh, F.; Srivatsan, S.; Andy, H. T. Macromolecules 2001, 34, 5902.
42. Göschel, U.; Swartjes, F. H. M.; Peters, G. W. M.; Meijer, H. E. H. Polymer 2000, 41, 1541.
43. Smith, J. V. X-Ray Powder Data File, American Society for Testing Materials: Philadelphia, PA, 1916.